Nuclear charge radii of the tin isotopes from muonic atoms

C. Piller, C. Gugler, R. Jacot-Guillarmod, L. A. Schaller,
L. Schellenberg, and H. Schneuwly
Physikinstitut der Universität Fribourg, CH-1700 Fribourg, Switzerland

G. Fricke, T. Hennemann, and J. Herberz
Institut für Kernphysik der Universität Mainz, D-6500 Mainz, Federal Republic of Germany
(Received 27 February 1990)

The muonic atom $2p_{1/2}$-$1s_{1/2}$ and $2p_{3/2}$-$1s_{1/2}$ transition energies were measured with an experimental accuracy of better than 20 ppm for the isotope chain ^{112,114,116,117,118,119,120,122,124}Sn. Precise values for the Barrett equivalent nuclear radii $R_{k\alpha}$ and their differences as well as root-mean-square radii were deduced. The $\Delta N=2$ isotope shifts between the even Sn isotopes show a subshell effect at the neutron number $N=64$. Otherwise, there is a nearly linear decrease with increasing N, in accordance with the general systematics of nuclear charge radii. Our muonic atom results are in a good agreement with recent optical data, including odd-even staggering. Hartree-Fock calculations reproduce the general trend but not the subshell effect. Regarding the nuclear polarization corrections, the problem in the $2p$ splitting found earlier in μ^--Zr and μ^--Pb seems also to persist in μ^--Sn.

I. INTRODUCTION

The nuclear charge radius is a fundamental quantity of each nucleus. It is not surprising that it has been one of the first nuclear properties investigated. However, its detailed behavior as a function of neutron or proton number is theoretically still not sufficiently understood.[1] Accurate experimental measurements, especially regarding changes of nuclear charge radii between neighboring isotopes or isotones, are thus of considerable interest. The present work is part of a collaboration between Los Alamos, Mainz, and Fribourg. Our aims are precision measurements of nuclear charge radii and their differences from light to medium-heavy nuclei, using the muonic-atom x-ray technique. In particular, the effects of shell and subshell structures can be tested when adding neutrons or protons within a series of isotopes or isotones.[2–4] Here, we present results on absolute nuclear charge radii as well as isotope shifts in tin ($Z=50$). From the $2p$-$1s$ muonic transition energies, we have obtained a precision of 2 am for the rms charge radii and of 1 am for the "model-independent" equivalent radii. The quoted errors include nuclear polarization uncertainties. Regarding the latter corrections, the tin data seem to corroborate the nuclear polarization anomaly found in the $2p$ levels.[5]

Tin is the element with the largest chain of stable isotopes (^{112}Sn-^{124}Sn). Since its proton number is magic, the effect of adding neutrons between the two major neutron shell closures at $N=50$ and 82, i.e., between $N=62$ and 74, can be studied without disturbing shell effects from the proton core. For instance, Hartree-Fock calculations can predict radial changes in such nuclei with rather high precision. Recently, laser-spectroscopic measurements of isotope shifts have been performed on tin atoms.[6,7] In particular, the isotope shifts between nuclei extending from ^{108}Sn up to ^{125}Sn have been studied. Such optical data over very long chains of isotopes, including unstable ones, can nicely describe the general trend of deformation within a major neutron shell. However, local variations, and especially subshell effects, are a strong-point of muonic atom measurements. In addition, in order to extract absolute nuclear charge radii, two optical constants must be known. In the present work, our muonic data on ^{112,114,116,117,118,119,120,122,124}Sn are compared with the optical data by means of a King plot, allowing an absolute calibration of the laser-spectroscopic results. Regarding charge radii differences, we can confirm the subshell effect after filling up the $1g_{7/2}$ neutron shell suggested by the optical measurements.

Section II deals with theory, i.e., with the different theoretical contributions that are necessary to evaluate the muonic-atom binding energies. Section III describes the experiment and presents a list of the experimental muonic $2p$-$1s$ energies measured in the investigated tin isotopes. Section IV treats the characteristics of nuclear charge parameters amenable in the muonic atom case. The results are presented in terms of "model-independent" equivalent nuclear charge radii $R_{k\alpha}$ and of root-mean-square (rms) charge radii $\langle r^2\rangle^{1/2}$, respectively. Their differences when adding pairs of neutrons as well as the so-called "odd-even" staggering effect between odd-even isotopes and the nuclear polarization in the $2p$ levels are discussed in Sec. V. Finally, Sec. VI compares our muonic atom results with the optical data in tin.

II. THEORY

The negative muon can be captured in the Coulomb field of a nucleus forming an "exotic atom". The capture state is usually a state of high quantum numbers n and l. In a heavier muonic atom, the following cascade process

TABLE I. Corrections to muonic binding energies for μ^--^{112}Sn. (For NP corrections see Table II). A positive correction means an increase in binding energy. Correction a, finite size binding energy correction b, vacuum polarization of the first order; correction c, vacuum polarization of second order; correction d, vacuum polarization of order equal or greater than 3; correction e, muonic and hadronic vacuum polarization; correction f, Lambshift, first, and second order vertex corrections; correction g, relativistic recoil and electron screening corrections.

	Correction (keV)						
State	a	b	c	d	e	f	g
$1s_{1/2}$	5250.061	36.213	0.296	−0.104	0.211	−1.826	0.230
$2p_{1/2}$	1814.917	10.510	0.078	−0.051	0.009	−0.028	0.026
$2p_{3/2}$	1768.936	9.773	0.072	−0.050	0.006	−0.108	0.023
$3d_{3/2}$	792.142	2.691	0.019	−0.022	0.000	+0.009	0.012
$3d_{5/2}$	786.168	2.615	0.018	−0.021	0.000	−0.006	0.012

down to the $1s$ ground state takes less than 10^{-14} s. The transitions occur preferentially between circular orbits $l=n-1$. While in low energy transitions between high n states Auger electrons are emitted, high energy transitions and particularly the $2p$-$1s$ transitions are dominated by electric dipole radiation.[8,9]

In order to calculate the muonic-atom transition energies, the Dirac equation has to be numerically solved, using an explicit form for the Coulomb potential and hence for the nuclear charge density $\rho(r)$. The usual "Ansatz" is a two-parameter Fermi distribution

$$\rho(r)=\frac{\rho_0}{1+\exp[(r-c)/a]}, \quad a=\frac{t}{4\ln 3} . \tag{1}$$

Here, the parameters c and t are the half-density radius and the skin thickness, respectively. Usually, the half-density radius c is varied when fitting the theoretical to the experimental transition energies. Due to the small $1s$ Bohr radii in muonic atoms, comparable to the nuclear charge radii in heavier nuclei, the influence of the finite nuclear charge extension on the muonic binding energies is considerable. This is called the finite-size effect. In ^{112}Sn, e.g., the point-nucleus binding energy of 7286 keV is lowered by 2027 keV or about 28% by the finite nuclear size. In precision measurements, further corrections to the Dirac point-nucleus energies must be applied before a comparison of experimental with theoretical transition energies can be made in order to determine the nuclear charge extension. These corrections are the QED corrections and the nuclear polarization corrections.[10] The largest QED contribution is the vacuum polarization. Its first order is smaller, roughly by the fine structure constant α, than the respective binding energy. Its potential is included as an additional term in the Coulomb potential before the Dirac equation is solved numerically. Higher-order vacuum polarization corrections, due to virtual $\mu^+\mu^-$ and hadronic pairs as well as self-energy corrections are treated in a perturbative way. In addition, relativistic recoil corrections[11] and electron screening corrections have to be applied.[12] The latter are treated by employing an additional potential V_e created by a mean electron density $\rho_e(r_e)$. The screening of the electrons increases slightly the muon binding energy. Table I lists the different QED corrections for the low-lying muonic-atom states of ^{112}Sn. If a precision of the order of 10 eV is demanded, all these corrections must be taken into account.

Regarding the so-called nuclear polarization (NP) corrections, they are much more difficult to calculate than QED corrections. By means of dynamic electromagnetic interactions, the muon can virtually excite the nucleus to higher states.[10] Such an effect reshuffles somewhat the eigenfunctions and hence the energy eigenvalues. Since the excitation spectra of nuclei are only insufficiently known, the NP corrections cannot be calculated to a high precision.[13] Typical errors are 20–30% for a given element and 10% when comparing different isotopes.[3,5] For the theoretical calculation of the *NP* corrections, we have employed the program MZMUON2, a modified version[14] of the computer code MUON2.[15] This program calculates the NP effect of the high-lying giant resonance states (HLS) using energy-weighted sum rules, while the energies and $B(E2)$ strengths of the discrete low-lying nuclear states (LLS) have to be taken from literature[16,17] and are fed in as input parameters. Table II shows the NP corrections for the $1s$ and the $2p$ states in the lightest and the heaviest measured Sn isotope.

III. EXPERIMENT

The experiment has been performed at the superconducting $\mu E1$ channel of the 590 MeV proton ring accelerator at the Paul Scherrer Institute (PSI) at Villigen. A proton beam of 100–200 μA produced π^- from a Be target. In three different running periods, either 220 or 150 MeV/c pion momenta were magnetically selected to produce backward decaying muons of 125 or 85 MeV/c, respectively. The muon beam intensity varied between

TABLE II. Nuclear polarization corrections (in eV) calculated from the low-lying states (LLS) and from the high-lying states (HLS). Only the values for ^{112}Sn and ^{124}Sn are reported because of their smooth A dependence, especially for the HLS.

Isotope		$1s_{1/2}$	$2p_{1/2}$	$2p_{3/2}$
^{112}Sn	HLS	1500	165	140
	LLS	255	90	86
^{124}Sn	HLS	1483	176	151
	LLS	246	79	76

TABLE III. Isotopic composition of the tin isotopes (in %).

Target	^{112}Sn	^{114}Sn	^{116}Sn	^{117}Sn	^{118}Sn	^{119}Sn	^{120}Sn	^{122}Sn	^{124}Sn
^{112}Sn	68.25	2.03	6.83	2.86	7.13	2.38	8.15	1.01	1.04
^{114}Sn	2.17	64.53	6.17	1.85	8.12	2.01	7.14		0.96
^{116}Sn			95.60	1.63	1.48	0.27	0.63		
^{117}Sn			2.54	84.23	9.40	1.24	2.03		
^{119}Sn			0.40	0.85	3.63	84.48	9.98	0.44	
^{120}Sn					0.61	0.66	98.05	0.34	
^{124}Sn					0.43	0.31	1.07	1.00	96.71

6×10^6 and 12×10^6 μ^-/s. After degrading, the muons were stopped in the different tin isotopes with thicknesses between 100 and 300 mg/cm^2. Table III lists the isotopic compositions of the employed isotopes.

With the exception of ^{112}Sn (metal), all other isotopes were in the form of SnO_2. The oxide powders were filled in thin plastic sacks and equally distributed over an area of 1.5×5 cm^2. Three different Sn isotopes could be measured simultaneously by a three-target setup, using separate scintillators of the appropriate target size in front of each of the three isotopes. The experimental arrangement is shown in Fig. 1.

The muonic x rays were measured using a 66 cm^3, intrinsic n-type Ge semiconductor detector. The energy spectra extended from about 0.1 to 4.2 MeV, with our main interest centered on the muonic ($2p$-$1s$) transitions. The resolution of the Ge diode (FWHM) was 2.0 keV at 1.33 MeV and 4.5 keV at 3.55 MeV at a counting rate of 5000/s. For some of the isotopes, a ^{56}Co source has been installed in a similar geometry and simultaneously measured for calibration purposes including nonlinearity measurements of the detection system. The main γ-ray energies and uncertainties of ^{56}Co have been taken from Ref. 18 (see Table IV). The data were stored in a PDP 11-34 computer employing the computer code DAVID.[19] The different 8 k spectra were divided into three categories, labeled "total," "prompt," and "delayed".

(a) In the total spectra, all events within a time span of 200 ns after a stopped muon are stored.

(b) In the prompt spectra, prompt (μ^-,γ) coincidences up to 20 ns after a stopped muon are measured. Such a narrow time window yields a spectrum of practically pure muonic x-rays. As an example, Fig. 2 shows on a logarithmic plot the $2p_{1/2}$-$1s_{1/2}$ and the $2p_{3/2}$-$1s_{1/2}$ transitions of the ^{116,120,124}Sn targets. Tails are due to isotopic impurities (see Table III).

(c) In the delayed spectra, delayed γ-rays from nuclear muon capture in a time interval of 30–200 ns after a stopped muon are recorded.

In the case of on-line calibrations (with ^{56}Co), the calibration lines appear by accidental coincidences (weakly) in the prompt and (strongly) in the delayed spectra. The precision of the line position is linearly dependent on the line width. Hence, energy resolution and line shape were controlled and, if necessary, readjusted after each measurement. In order to avoid line broadening by electronic or temperature-dependent shifts, the different spectra were written on tape every 4–6 h. For sufficient statistics, a large number of such spectra had to be recorded. About 10% of all spectra showed a line broadening of more than 5%. Those were therefore discarded. In each of the remaining "good" spectra, the positions of two strong lines were compared and, if necessary, shifted. Afterwards, the different spectra were added to yield a total histogram.

For the analysis of the line shapes and the determination of the center of gravity line positions, the computer code MYFIT (Ref. 20) was employed. This program utilizes basically a Gaussian function. If necessary, exponential tails may be added and the Lorentzian natural line shape may be folded in.

Regarding the nonlinearity of our measuring system, off- and on-line calibrations with ^{56}Co have been performed. All these spectra show a similar nonlinearity structure. The small deviations from linearity were fitted by a smooth curve in the energy region of interest and the corresponding corrections were applied to the center-of-gravity positions of all our prompt and delayed spectra. The overall uncertainty of the nonlinearity curve was es-

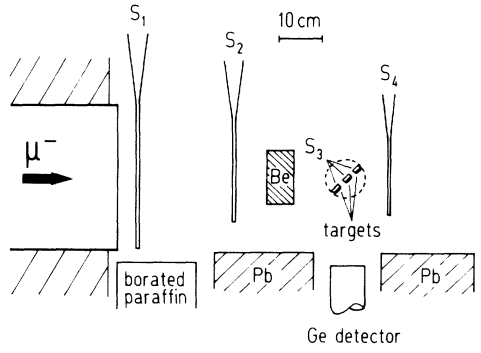

FIG. 1. Experimental setup used at PSI for our tin measurements. S_1, S_2, S_3, and S_4 are thin plastic scintillators.

TABLE IV. ^{56}Co γ-ray energies used for calibration.

Source	Energies (keV)		
^{56}Co	846.764(6)	1037.844(4)	1175.099(8)
	1238.287(6)	1360.206(6)	1771.350(15)
	1963.714(12)	2015.179(11)	2034.759(11)
	2598.460(10)	3009.596(17)	3201.954(14)
	3253.417(14)	3272.998(14)	3451.154(13)

timated to be 15 eV. As for the absolute energy calibration of our measured muonic x-ray transitions, the ^{56}Co lines in the delayed spectra were used. Such an on-line procedure assures practically the same experimental conditions as for the prompt spectra. Still, a small shift between prompt and delayed spectra is possible due to nonidentical timing conditions. By applying the above-mentioned line fitting and energy calibration procedures and by adding the respective nuclear recoil corrections (e.g., 54 eV for the 2p-1s transitions in μ^--^{112}Sn), the transition energies for the Sn isotopes ^{112,114,116,117,119,120,124}Sn listed in Table V have been obtained.

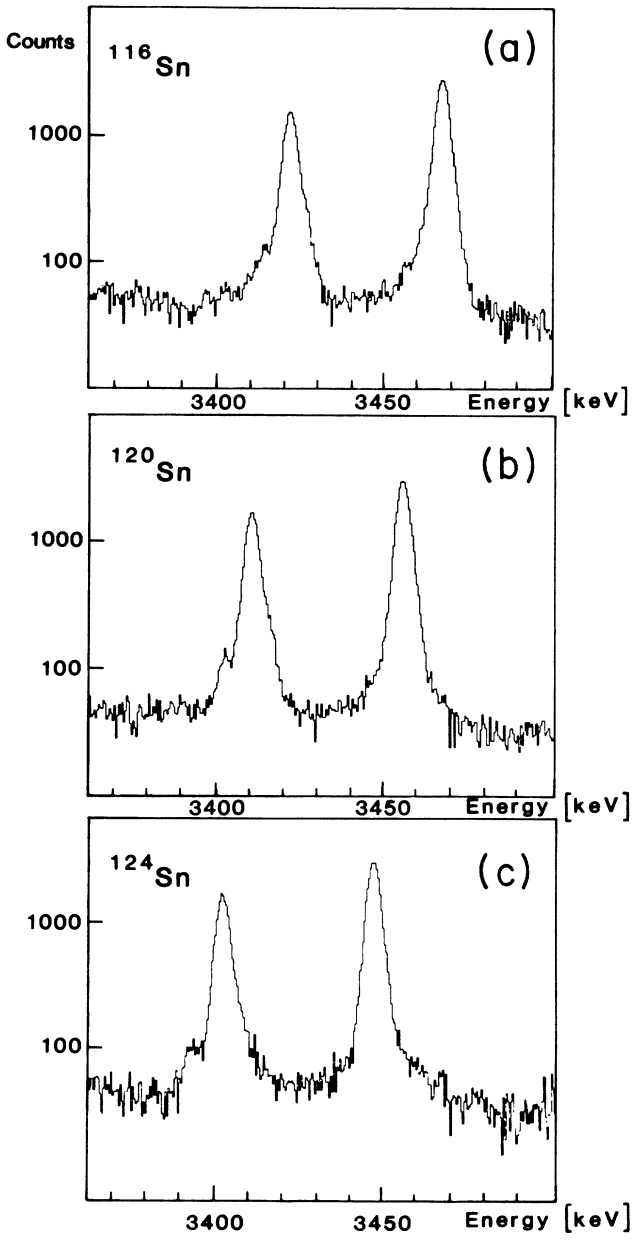

FIG. 2. Prompt muonic x-ray spectra showing the $2p_{1/2}$-$1s$ and the $2p_{3/2}$-$1s$ transitions in ^{116}Sn (a), ^{120}Sn (b), and ^{124}Sn (c).

IV. NUCLEAR CHARGE RADII AND ISOTOPE SHIFTS

If we select a nuclear charge density $\rho(r)$ like the one given in Sec. II, the experimental transition energies can be fitted to the calculated ones and nuclear rms charge radii can be extracted. In general, both the $2p$-$1s$ and the $3d$-$2p$ transitions have been included in the fit. In order to obtain high accuracies, one should employ the differences $\Delta V_{if}(r)$ of the muon potentials in the initial (i) and final (f) state, which, as Barrett has shown,[21] are practically independent of the charge density:

$$\Delta V_{if}(r) = A + Br^k e^{-\alpha r} . \tag{2}$$

The parameters A and B are normalization parameters. The parameter k depends on the chosen transition, but shows only a weak Z dependence, while the parameter α is practically the same for different transitions but depends nearly linearly on Z. In our analysis, we have varied B, k, and α to obtain a best fit for each transition. Each muonic transition energy determines a model-independent radial moment, the so-called Barrett moment. For a spherically symmetric nucleus, this moment becomes

$$\langle r^k e^{-\alpha r} \rangle = 4\pi \int_0^\infty \rho(r) r^k e^{-\alpha r} r^2 dr . \tag{3}$$

Instead of the Barrett moment, we can define a more transparent quantity, namely the so-called equivalent radius $R_{k\alpha}$, which means the radius of a homogeneously charged sphere yielding the same Barrett moment $\langle r^k e^{-\alpha r} \rangle$:

$$3R_{k\alpha}^{-3} \int_0^{R_{k\alpha}} r^k e^{-\alpha r} r^2 dr = \langle r^k e^{-\alpha r} \rangle . \tag{4}$$

The sensitivity of $R_{k\alpha}$ with respect to a change in the transition energy is given by the quantity

$$C_z = -\frac{dR_{k\alpha}}{dE} = -R_{k\alpha}[3Ze^2 B(\langle r^k e^{-\alpha r} \rangle - R_{k\alpha}^k e^{-\alpha r})]^{-1} . \tag{5}$$

The error of $R_{k\alpha}$ is calculated from the error of the transition energies. After adapting the Fermi charge distribution parameter c in order to obtain the measured transition energies (using a constant skin thickness parameter $t = 2.30$ fm), we can calculate the values for k and α from the muon potentials. Finally, in order to compare our $R_{k\alpha}$ and rms radii for the different isotopes,

TABLE V. Experimental muonic transition energies in keV (recoil corrected). The errors include statistical and calibration uncertainties.

Isotope	$2p_{1/2}$-$1s_{1/2}$	$2p_{3/2}$-$1s_{1/2}$
^{112}Sn	3432.564±0.060	3478.531±0.056
^{114}Sn	3426.613±0.071	3471.921±0.068
^{116}Sn	3420.091±0.062	3465.757±0.058
^{117}Sn	3418.140±0.063	3463.810±0.060
^{119}Sn	3412.848±0.061	3458.780±0.060
^{120}Sn	3408.975±0.052	3454.453±0.050
^{124}Sn	3400.182±0.061	3445.482±0.057

TABLE VI. Nuclear charge parameters deduced from the muonic $2p$-$1s$ transitions in the Sn isotopes. The quoted errors correspond to the experimental uncertainties.

Isotope	$R_{k\alpha}$ (fm)	$\Delta R_{k\alpha}$ (am)	rms (fm)	Δrms (am)
^{112}Sn	5.8803±0.0002		4.5958±0.0005	
		18.9		14.5
^{114}Sn	5.8992±0.0002		4.6103±0.0005	
		20.6		15.8
^{116}Sn	5.9198±0.0002		4.6261±0.0005	
		17.7		13.4
^{118}Sn	5.9375±0.0002		4.6395±0.0005	
		16.5		12.7
^{120}Sn	5.9540±0.0002		4.6522±0.0006	
		14.5		11.1
^{122}Sn	5.9685±0.0002		4.6633±0.0006	
		13.5		10.3
^{124}Sn	5.9820±0.0002		4.6736±0.0006	
^{117}Sn	5.9242±0.0003	16.9	4.6320±0.0006	12.8
^{119}Sn	5.9411±0.0003		4.6448±0.0006	

we have to use the same values of k and α for the same transitions. Table VI shows the nuclear charge parameters $R_{k\alpha}$ and $\langle r^2\rangle^{1/2}$ (in fm) together with their differences $\Delta R_{k\alpha}$ and $\Delta\langle r^2\rangle^{1/2}$ (in am) for all measured tin isotopes. The upper part shows these differences for the even isotopes, the lower part for the odd ones. The average values for k and α are $k=2.1762$ and $\alpha=0.1076$/fm. The data for ^{118}Sn and ^{122}Sn are taken from a former run at Los Alamos, where the isotope shifts $^{120-118}$Sn and $^{122-120}$Sn were measured. The absolute radii are normalized to our ^{120}Sn measurements.

V. DISCUSSION OF THE NUCLEAR CHARGE PARAMETERS

In Fig. 3, we represent graphically the equivalent nuclear charge radii differences

$$\Delta R_{k\alpha}^{A,A+2}=R_{k\alpha}(A+2)-R_{k\alpha}(A) \quad (6)$$

between all even, stable Sn isotopes, drawn in at the mass number $A+1$. The uncertainties contain, besides the experimental error, a 10% theoretical uncertainty due to nuclear polarization.

With the exception of the results at $A=115$ ($N=65$), the radii differences drop almost linearly with increasing neutron numbers. Such an effect is expected from the systematics of nuclear charge radii within major neutron shells.[2-4] In the case of tin, the $N=50$ shell is completed, and the $N=82$ shell is about halfway filled. The fact that the Los Alamos radii differences ($\Delta R_{k\alpha}^{118,120}$ and $\Delta R_{k\alpha}^{120,122}$) fall smoothly between the PSI results corroborates the experimental consistency at the two different laboratories. Looking at the subshells, at $N=64$ both the $2d_{5/2}$ and the $1g_{7/2}$ subshells are filled. Hence, the additional two neutrons in $^{116}Sn_{66}$ must occupy a new subshell, probably the $1h_{11/2}$ shell. Since the proton charge distribution is then moved more outwards than within a

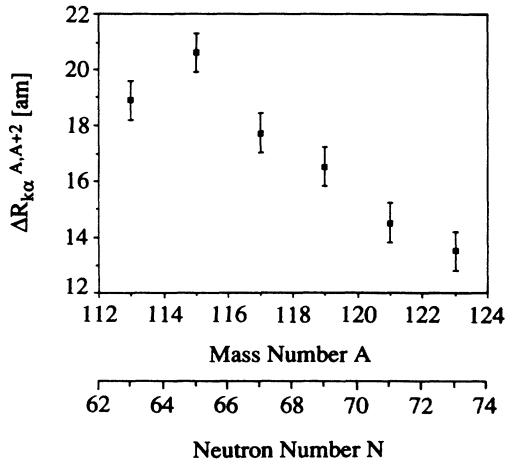

FIG. 3. Charge radii differences $\Delta R_{k\alpha}^{A,A+2}$ of the even Sn isotopes (in units of am) as a function of mass number A, or neutron number N, respectively. The values are plotted at $A+1$ ($N+1$).

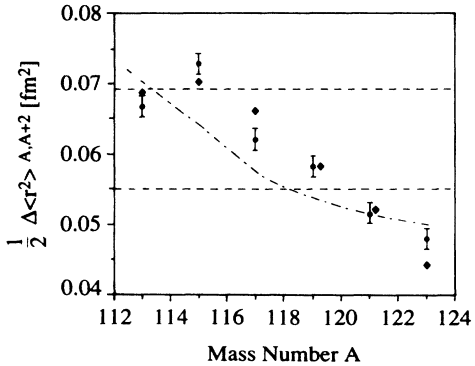

FIG. 4. Brix-Kopfermann diagram. Plotted are the differences $\frac{1}{2}\Delta\langle r^2\rangle^{A,A+2}$ as a function of the mass number A, drawn in at $A+1$. Our results are presented with experimental errors. Also shown are optical data (black diamond) as well as theoretical predictions (see text).

subshell, the radius difference $\Delta R_{k\alpha}^{114,116}$ becomes larger than the preceding difference $\Delta R_{k\alpha}^{112,114}$, which lies within the $1g_{7/2}$ subshell. The result at $N=65$ therefore confirms the subshell effect suggested by the optical data[6] and already seen in the even Cd isotopes[22] for the same number of neutrons.

Instead of plotting the equivalent charge radii differences, our data can be presented in a form more amenable to theory and to a comparison with optical results. For this purpose, we show in Fig. 4 a so-called Brix-Kopfermann diagram, where half the difference of our rms radii $\langle r^2\rangle$ between adjacent even Sn isotopes

$$\tfrac{1}{2}\Delta\langle r^2\rangle^{A,A+2}=\tfrac{1}{2}(\langle r^2\rangle^{A+2}-\langle r^2\rangle^{A}) \tag{7}$$

is plotted against the mass number A.

The errors in Fig. 4 are experimental. The diagram also shows the optical data of Eberz *et al.*[7] in the form of black diamonds, without errors. The optical uncertainties are about 2–3 times larger than ours. Since the results of Ref. 7 have been calibrated by the old muonic atom data of Ref. 23, we have corrected them by 3.2% using our value $\Delta\langle r^2\rangle^{116,124}=0.4417(23)$ fm^2. Regarding theory, Myers droplet model and refinements thereof yield only a horizontal line in the differential Brix-Kopfermann plot, with values between 0.055 fm^2 (Ref. 24) and 0.068 fm^2 (Ref. 25). The two limits are indicated by dashed lines in Fig. 4. On the other hand, Hartree-Fock calculations including ground state correlations and the density-dependent Skyrme force[26] G_σ also show differential structure but fail to reproduce the subshell effect (see Fig. 4, dashed-dotted line). In addition, such radii differences based on microscopic calculations are generally smaller than the experiment, at least in the region of the stable Sn isotopes. According to Ref. 6 there are nuclear structure calculations based on the Hartree-Fock-Bogoliubov (HFB) theory, which seem to predict a dip in the region of interest, but shifted by one unit on the mass scale.[27]

As of now, we have dealt with the effects of adding pairs of neutrons. However, we have also measured the nuclear charge radii of the odd tin isotopes ^{117}Sn and ^{119}Sn (see Table VI). If we look at the radii differences between these odd-N isotopes and the neighboring even ones, the influence of the unpaired neutron can be seen. This effect is usually expressed by the odd-even staggering parameter[28]

$$\gamma(A+1)=\frac{R_{k\alpha}(A+1)-R_{k\alpha}(A)}{\frac{1}{2}[R_{k\alpha}(A+2)-R_{k\alpha}(A)]}\ . \tag{8}$$

A $\gamma<1$ means that the odd neutron isotopes have smaller charge radii than the average of their even-neutron neighbors. In other words, the proton core polarization effect from the unpaired neutron is smaller than half the proton core polarization due to paired neutrons. Table VII shows that the staggering parameter both for the ^{118,117,116}Sn and the ^{120,119,118}Sn cases is below 0.5.

On the theoretical side, the primary cause for odd-even staggering seems to be the pairing force. If, in a HFB calculation, the pairing strength of the neutrons is coupled to the single particle potential of the protons and thus to the charge radii, the odd-even "fine-structure" of the tin charge radii can be roughly reproduced. Still, the calculated odd-even staggering turns out to be more uniform than in the experiment.[1]

To conclude this section, we briefly return to the nuclear polarization corrections. As already stated in Sec. II, these calculations limit the accuracy with which nuclear charge radii can be extracted from the measurements. In two recent publications,[29,30] an inversion in magnitude of the nuclear polarization (NP) corrections for the two $2p$ states must be assumed to bring experiment and theory into accordance. If we now compare experimental and fitted energies for both the $2p_{1/2}$-$1s$ and the $2p_{3/2}$-$1s$ transitions, the calculated $2p$ fine structure splittings $\Delta(2p)$ in all measured Sn isotopes are consistently too high (of the order of 150 eV). If the reason for these deviations are the nuclear polarization calculations in the two $2p$ levels, where the difference

$$\Delta\mathrm{NP}(2p)=\mathrm{NP}(2p_{1/2})-\mathrm{NP}(2p_{3/2}) \tag{9}$$

is positive, then a sign reversal would again yield better agreement with experiment. Hence, a fundamental problem in present approaches to the calculation of the nuclear polarization effects seems to persist also for the tin nuclei.

VI. COMPARISON WITH OPTICAL DATA

In the differential Brix-Kopfermann plot of the preceding section, we have already presented the laser spectroscopy measurements of Eberz *et al.*[7] corrected by our $\Delta\langle r^2\rangle^{116,124}$ value. As can be seen from Fig. 4, there is good agreement between the optical data and our muonic atom results. In the following, we compare our muonic tin data with the optical data of Refs. 6 and 7 by means of two King plots.[31] Such a plot allows in particular a precise determination of the electron density at the nucleus, a quantity which can only be determined with large errors from optical data alone. The experimental optical frequency shifts $\Delta\nu^{AA'}$ are in a good approximation a linear function of the radii differences $\Delta\langle r^2\rangle^{AA'}$. In fact,

$$\Delta\nu^{AA'}=F\lambda'^{AA'}+M(A'-A)/A'A\ , \tag{10}$$

TABLE VII. Staggering parameters for ^{117}Sn and ^{119}Sn.

Isotopes	$\Delta R_{k\alpha}$ (am)	Isotopes	γ
^{117}Sn–^{116}Sn	4.4		
^{118}Sn–^{117}Sn	13.3	^{118}Sn–^{117}Sn–^{116}Sn	$\gamma(117)=0.497(23)$
^{119}Sn–^{118}Sn	3.6		
^{120}Sn–^{119}Sn	12.9	^{120}Sn–^{119}Sn–^{118}Sn	$\gamma(119)=0.436(33)$

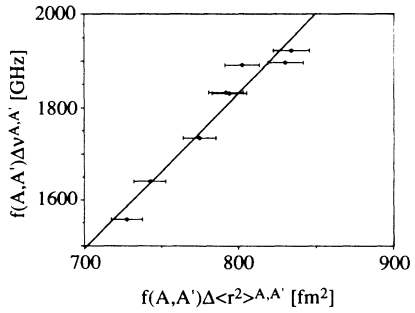

FIG. 5. King plot between the $\lambda=286.3$ nm optical data of Ref. 6 and our muonic data. The reference isotope (A') is ^{124}Sn.

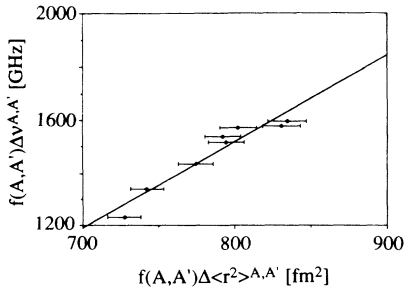

FIG. 6. King plot between the $\lambda=452.5$ nm optical data of Ref. 7 and our muonic data. The reference isotope (A') is ^{124}Sn.

where

$$\lambda'^{AA'}=\Delta\langle r^2\rangle^{AA'}+c_2/c_1\Delta\langle r^4\rangle^{AA'}+\cdots , \quad (11)$$

$$M=N+S , \quad (12)$$

$$N=\nu m_e/m_p=(c/\lambda)m_e/m_p . \quad (13)$$

In these relations, F is the difference in electron density at the nucleus for the two levels of the transition, N is the normal mass shift, S is the specific mass shift, $\nu=c/\lambda$ is the frequency of the chosen transition, m_e is the electron mass, m_p is the proton mass and the c_i's are the coefficients of Seltzer.[32] The second term in the expression for $\lambda'^{AA'}$ contributes less than 4% in the tin isotopes and is accounted for when calibrating the optical data with a muonic $\Delta\langle r^2\rangle$ value. Hence, it can be neglected. If muonic atom data are included, the King plot compares the muonic rms radii differences $\Delta\langle r^2\rangle^{AA'}$ plotted on the x axis with the optical isotope shifts $\Delta\nu^{AA'}$ for a given transition plotted on the y axis. Both data are normalized by the factor

$$f(A,A')=AA'/(A'-A) . \quad (14)$$

With consistent data sets, a straight line should result. As can be seen from Figs. 5 and 6, this is indeed the case for both the $\lambda=286.3$ nm transition from Ref. 6 and the $\lambda=452.5$ nm data from Ref. 7.

The parameters F are determined as $F=3.35(20)$ GHz/fm^2 for $\lambda=286.3$ nm and $F=3.29(20)$ GHz/fm^2 for $\lambda=452.5$ nm. Regarding odd-even staggering, Anselment *et al.*,[6] following a suggestion by Talmi, define as an absolute measure of this effect the quantity [note that the second expression of Eq. (5) in Ref. 6 contains the wrong sign]

$$\Delta=\langle r^2\rangle^A-(\tfrac{1}{2}\langle r^2\rangle^{A-1}+\tfrac{1}{2}\langle r^2\rangle^{A+1})$$
$$=\tfrac{1}{2}(\Delta\langle r^2\rangle^{A-1,A}+\Delta\langle r^2\rangle^{A+1,A}) . \quad (15)$$

Inserting our values for the neighboring isotopes ^{117,118,119}Sn, we obtain

$$\Delta(A=117)=-0.012(2)\ \text{fm}^2 ,$$

$$\Delta(A=118)=+0.010(2)\ \text{fm}^2 ,$$

$$\Delta(A=119)=-0.010(2)\ \text{fm}^2 .$$

These results agree, within the uncertainties, with the optical values given in Ref. 6.

ACKNOWLEDGMENTS

The authors wish to acknowledge particularly the contributions of Dr. E. B. Shera and Dr. M. V. Hoehn to this work by providing them with the $\Delta R_{k\alpha}$ values of ^{118,120}Sn and ^{120,122}Sn measured at Los Alamos. They are also indebted to them for the loan of the ^{112}Sn isotope. For one of us (C. P.), this work was part of the requirements for his Ph.D. thesis. Finally, the authors would like to thank the Swiss National Foundation for financial support.

[1]U. Regge and D. Zawischa, Comments At. Mol. Phys. **23**, 5 (1989).

[2]L. Schellenberg, B. Robert-Tissot, K. Käser, L. A. Schaller, and H. Schneuwly, Nucl. Phys. **A333**, 333 (1980).

[3]L. A. Schaller, D. Barandao, P. Bergem, M. Boschung, T. Q. Phan, G. Piller, A. Rüetschi, L. Schellenberg, and H. Schneuwly, Phys. Rev. C **31**, 1007 (1985).

[4]E. B. Shera, M. V. Hoehn, G. Fricke, and G. Mallot, Phys. Rev. C **39**, 195 (1989).

[5]L. A. Schaller, in *Proceedings of the International Symposium on Dynamics of Collective Phenomena in Nuclear and Subnuclear Long-Range Interactions in Nuclei, Bad Honnef, 1987* (World Scientific, Singapore, 1988), p. 145.

[6]M. Anselment, K. Bekk, A. Hanser, H. Hoeffgen, G. Meisel, S. Göring, H. Rebel, and G. Schatz, Phys. Rev. C **34**, 1052 (1986).

[7]J. Ebertz, U. Dinger, G. Huber, H. Lochmann, R. Menges, G. Ulm, R. Kirchner, O. Klepper, T. U. Kühl, and D. Marx, Z. Phys. A **326**, 121 (1987).

[8]R. Jacot-Guillarmod, F. Bienz, M. Boschung, C. Piller, L. A. Schaller, L. Schellenberg, H. Schneuwly, and D. Siradovic, Phys. Rev. A **37**, 3795 (1988).

[9]F. Scheck, *Leptons, Hadrons and Nuclei* (North-Holland, Amsterdam, 1983).

[10]E. Borie and G. A. Rinker, Rev. Mod. Phys. **54**, 67 (1982).
[11]J. L. Friar and J. W. Negele, Phys. Lett. **B46**, 5 (1973).
[12]J. B. Mann and G. A. Rinker, Phys. Rev. **A11**, 385 (1975).
[13]G. A. Rinker and J. Speth, Nucl. Phys. **A306**, 397 (1978).
[14]G. Mallot and T. Hennemann Mainz, private communication.
[15]Y. Tanaka, The formalism of MUON2 and XRAY2, Los Alamos report, 1984 (unpublished).
[16]P. M. Endt, At. Data Nucl. Data Tables **26**, 47 (1981).
[17]S. Raman, C. H. Malarkey, W. T. Milner, C. W. Nestor, Jr., and P. H. Stelson, At. Data Nucl. Data Tables **36**, 1 (1987).
[18]R. G. Helmer, P. H. M. Van Assche, and C. Van der Leun, At. Data Nucl. Data Tables **24**, 39 (1979).
[19]W. Reichart, Computer Code DAVID, Zürich (unpublished).
[20]G. Mallot, Mainz, private communication.
[21]R. C. Barrett, Phys. Lett. **B33**, 388 (1970).
[22]R. Wenz, A. Timmermann, and E. Matthias, Z. Phys. A **303**, 87 (1981).
[23]R. B. Chelser and F. Boehm, Phys. Rev. **166**, 1206 (1968).
[24]W. D. Myers and K. H. Schmidt, Nucl. Phys. **A410**, 61 (1983).
[25]D. Berdichevsky, R. Fleming, D. W. L. Sprung, and F. Tondeur, Z. Phys. A **329**, 393 (1988).
[26]J. Friedrich and P. G. Reinhard, Phys. Rev. C **33**, 335 (1986).
[27]J. Dobaczewski, M. Flocard, and J. Treiner, Nucl. Phys. **422**, 103 (1984).
[28]E. B. Shera, E. T. Ritter, R. B. Perkins, G. A. Rinker, L. K. Wagner, H. D. Wohlfahrt, G. Fricke, and R. M. Steffen, Phys. Rev. C **14**, 731 (1976).
[29]P. Bergem, C. Piller, A. Rüetschi, L. A. Schaller, L. Schellenberg, and H. Schneuwly, Phys. Rev. C **37**, 2821 (1988).
[30]T. Q. Phan, P. Bergem, A. Rüetschi, L. A. Schaller, and L. Schellenberg, Phys. Rev. C **32**, 609 (1985).
[31]W. H. King, *Isotope Shifts in Atomic Spectra* (Plenum, New York, 1984).
[32]E. C. Seltzer, Phys. Rev. **188**, 1916 (1969).